

Research Article

Robust Controller Design for a Grid-Connected VSI via an LCL Filter in the Presence of Unknown Grid Impedance

Juan Manuel Gonzalez^{1*}, Claudio A. Busada², Jorge A. Solsona²

¹Instituto Argentino de Radioastronomía (IAR), Universidad Nacional de La Plata (UNLP)-CONICET, Berazategui, Argentina

²Instituto de Investigaciones en Ingeniería Eléctrica (IIIE), Universidad Nacional del Sur (UNS)-CONICET, Bahía Blanca, Argentina
E-mail: jmgonzalez@iar.unlp.edu.ar

Received: 11 September 2024; **Revised:** 13 November 2024; **Accepted:** 18 November 2024

Abstract: Inverters connected to the grid can become unstable under specific grid impedance conditions. In order to find a solution to this problem, it is possible to ensure system stability and their robustness to R-L type grid impedances by satisfying two conditions. The first condition is to ensure that the closed-loop poles of the system are in stable positions to variations in the grid impedance. The second condition is reliant on the admittance model of the equivalent circuit. Specifically, the product of this admittance and the grid impedance must adhere to the Nyquist stability criterion. In this work, the stability of the converter connected to the grid through an LCL filter is analysed. For this purpose, the output admittance is modelled in the Laplace domain taking into account the behaviour of the discrete controller. In addition, to ensure that the closed-loop poles are in stable positions, the system open-loop response is analysed. These two conditions are examined across scenarios where system states are partially or completely fed back, for different system parameter values. Consequently, a robust controller is designed for variations of the R-L type grid impedance.

Keywords: grid-connected inverter, weak grid, output admittance, robustness

Abbreviation

Abbreviation	Description
VSI	Voltage Source Inverter
PCC	Point of Common Coupling
T_s	Sampling time (s)
ω_s	Sampling angular frequency (rad/s)
δ	Dirac delta function
\vec{v}_g	Grid voltage source (V)
Z_g	Grid impedance (Ω)
v_{dc}	DC voltage source (V)
\vec{v}_{ref}	Reference control signal (V)
\vec{v}_i^*	One-sample delayed signal (V)
\vec{v}_i	Signal applied to LCL filter input (V)

\vec{v}_s	Voltage at PCC (V)
\vec{i}_i	Current through L_i (A)
\vec{i}_s	Current through L_s (A)
\vec{v}_c	Voltage across C (V)
L_i	Inverter side inductance (H)
L_s	Grid side inductance (H)
C	Filter capacitor (F)
$\mathbf{Y}_o(s)$	Admittance of the output filter (S)
z^{-1}	One-sample delay
$\mathbf{R}(z)$	Reference prefilter
$\mathbf{C}(z)$	Feedback controller
$\mathbf{C}_1(z)$	Feedback gain for \vec{i}_i
$\mathbf{C}_2(z)$	Feedback gain for \vec{v}_c
$\mathbf{C}_3(z)$	Feedback gain for \vec{i}_s
PI	Proportional-integral controller
PR	Proportional-resonant controller
$\mathbf{C}_4(z)$	Feedback gain for \vec{v}_i
$\mathbf{G}_h(s)$	Zero-order hold (ZOH)
$\mathbf{I}_{i1}(s)$	Transfer function of current through L_i with respect to v_i
$\mathbf{I}_{i2}(s)$	Transfer function of current through L_i with respect to v_s
$\mathbf{V}_{c1}(s)$	Transfer function of voltage across C with respect to v_i
$\mathbf{V}_{c2}(s)$	Transfer function of voltage across C with respect to v_s
$\mathbf{I}_{s1}(s)$	Transfer function of current through L_s with respect to v_i
$\mathbf{I}_{s2}(s)$	Transfer function of current through L_s with respect to v_s
$\Delta_i(z)$	Transfer function numerator for $\mathbf{I}_{i1}(z)$
$\Delta_c(z)$	Transfer function numerator for $\mathbf{V}_{c1}(z)$
$\Delta_s(z)$	Transfer function numerator for $\mathbf{I}_{s1}(z)$
$\Delta_r(z)$	Characteristic polynomial in Z domain
ω_r	Resonance angular frequency (rad/s)
ω_{ari}	Anti-resonance angular frequency (rad/s)
L_T	Total inductance (H)
ω_{crit}	Critical angular frequency (rad/s)

1. Introduction

The increasing demand for energy has driven the expansion of renewable energy sources, leading to the development of power electronic converters capable of injecting energy into the grid. Consequently, inverter-based resources (IBRs) have emerged, where electrical variables need to be controlled and synchronized [1]. Primarily, two control strategies are utilized: in some cases, the converters operate as grid-forming and in others as grid-feeding [2, 3]. The design of these controllers is based on the knowledge of parameters at the Point of Common Coupling (PCC) and assuming that the voltage at this point matches the grid voltage. Sometimes the converter is connected to the grid through a line with unknown parameters. Depending on the short-circuit ratio (SCR), two clearly distinguishable scenarios arise. In one case, the grid can be considered strong, and the performance of the employed controller is not affected. On the contrary, when the grid is weak, the system's performance may deteriorate, potentially leading to unstable behavior [4, 5, 6, 7, 8].

In many cases, renewable energy sources are integrated into the grid using grid-feeding inverters [9]. These inverters incorporate a passive filter as an output stage to attenuate the harmonic components generated by the PWM modulator. Typically, either an L filter or an LCL filter is employed. Sometimes, the LCL filters are preferred due to their ability to create a smaller filter than an L filter for the same attenuation factor. However, LCL filters exhibit resonant behavior,

making it challenging to control the injected current. To address this, various methods, categorized as passive damping [10, 11] or active damping [12, 13], have been proposed. Passive damping introduces power losses, impacting efficiency, thus making active damping more preferable. This article assumes the use of an LCL filter as the grid-feeding output stage.

As the grid impedance value is unknown and subject to variations, so is the resonant frequency of the impedance formed by the LCL filter and the grid impedance. Therefore, ensuring stability involves designing controllers that are robust to variations in the grid impedance.

To address these challenges, several control methods have been developed that analyse the open-loop response of the system, allowing for the determination of the stability of closed-loop poles [14, 12]. Controllers with converter side current feedback exhibit instability when the resonance frequency surpasses one-sixth of the sampling frequency [14]. In contrast, for controllers with grid current feedback, instability arises when the resonant frequency falls below one-sixth of the sampling frequency [12]. To enhance system robustness to variations in grid impedance, controllers with a second inner current loop were developed [12, 15]. However, certain resonant frequency values may still lead to instability. To address this, a phase compensator was introduced in [15]. Additionally, the application of full-state feedback controllers enhances system robustness within a limited range of grid impedance values. A robust design of an observer-based current controller, considering a converter connected to a weak grid through an LCL filter, was proposed in [16, 17, 18]. Further proposals, which involve robust H_∞ control, can be found in [19].

On the other hand, the grid-connected inverter can be modelled as a current source in parallel to an admittance, ensuring system stability if the product between the inverter output admittance and the grid impedance satisfies the Nyquist stability criterion [20, 21, 22]. If the LCL filter parameters are known, the inverter output admittance can be modelled, offering the advantage of evaluation across the entire frequency range.

Usually, the output admittance of a converter is modelled by considering the system in continuous time [23, 24, 25, 21, 22]. However, the controller is implemented digitally, with equations in the discrete domain. Due to this, the system can be considered as a mixed-domain system, consisting of continuous and discrete-time signals. It must be noted that, purely continuous-time models may give erroneous results, in particular for low sampling frequencies [26]. In addition, not all digital control algorithms can be accurately modelled using continuous-time transfer functions. To improve the accuracy of the admittance model, the discrete behaviour of the control system is considered, maintaining the continuous characteristic of the rest of the system [27]. Likewise, there are purely discrete models of the output admittance [28, 29]. However, these models do not accurately describe the output admittance, especially at frequencies near or above the Nyquist frequency. On the other hand, in most admittance modelling methods, the sampling process is not taken into account. Such a process is considered in recent work, where sampling is modelled as intermodulation products [26, 30, 31].

However, to design a controller robust to variations in a grid impedance of the R-L type, it is necessary to meet both conditions. The closed-loop poles must remain in stable positions despite variations in the grid impedance, and the product of the grid impedance and the system admittance must satisfy the Nyquist stability criterion [22, 32]. Usually, it is only proposed that the system be stable for one of the conditions and not both. This paper introduces the analysis of the output admittance model for a controller by considering two different cases (i.e., partial-state or full-state feedback). Models are developed in the Laplace domain considering the behaviour of the discrete-time controller. In addition, the open-loop response of the system is analysed to ensure that the closed-loop poles are located in positions such as system stability is guaranteed. The open loop is considered with all loops closed except for the output current loop. This analysis allows the design of a controller robust to variations in the grid impedance of the R-L type. Thus achieving the design of a controller that satisfies both stability criteria.

The paper is organized as follows. Section 2 describes the system under study. Section 3 analyses the system stability and its relation with the output admittance. Section 4 develops the admittance model and the open-loop response of the system when different states are fed back. Furthermore, the extension of the model to a three-phase system is outlined, considering the dynamics of the phase-locked loop (PLL). Finally, Sections 5 and 6 present the simulation results and conclusions, respectively.

2. System description

This section describes the configuration of an inverter (VSI) connected to the grid through an LCL filter. This is shown in Figure 1, where L_i and L_s represent the inverter and grid-side inductances, respectively, and C is the filter capacitor. The inverter is modelled with a unity gain and \vec{v}_i denotes the inverter output voltage. We denote \vec{i}_i as the current on the inductor L_i , \vec{i}_s as the current on the inductor L_s and \vec{v}_c as the voltage on the capacitor C . The grid is modelled as an ideal voltage source \vec{v}_g in series with an impedance Z_g . The voltage over the coupling point (PCC) is denoted as \vec{v}_s . The control signal to be applied is denoted as \vec{v}_{ref} and \vec{v}_i^* is the voltage applied to the inverter. We assume the one-sample processing delay between the \vec{v}_{ref} and \vec{v}_i^* signal, represented by the z^{-1} block [33].

Figure 2 shows the Norton equivalent circuit of the VSI with LCL output filter connected to the grid. There the converter is modelled as a current source \vec{I} in parallel to an admittance $Y_o(s)$.

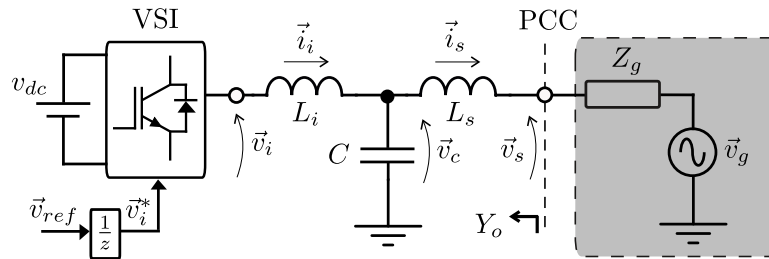


Figure 1. Schematic model of inverter connected to the grid through an LCL filter. The grid is modelled as a voltage source \vec{v}_g in series with an impedance Z_g . The inverter is represented as the VSI block, the supply voltage source as v_{dc} , the control signal as \vec{v}_{ref} , \vec{v}_i^* as the one-sample delayed signal, and \vec{v}_i as the signal applied to the LCL filter input. \vec{v}_s is the voltage at the PCC, \vec{i}_i the current through L_i , \vec{i}_s the current through L_s , and \vec{v}_c the voltage across C .

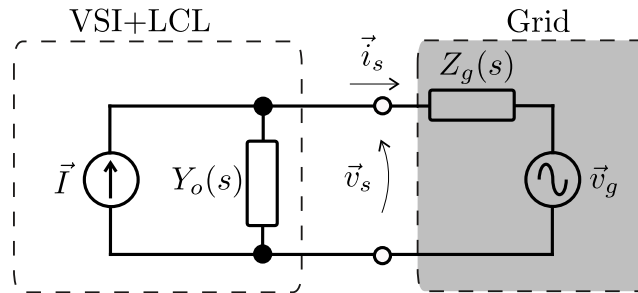


Figure 2. Norton equivalent circuit of the VSI with LCL output filter connected to the grid. The converter is modelled as a current source \vec{I} in parallel to an admittance $Y_o(s)$. The grid is modelled as an ideal voltage source \vec{v}_g in series with a grid impedance $Z_g(s)$. The voltage at PCC is \vec{v}_s and the grid current \vec{i}_s .

3. Admittance modelling for full feedback states

This section models the output admittance for full feedback states, also presenting the open-loop transfer function of the system response. Figure 3 illustrates the schematic diagram of the controller with full state feedback, where the switches represent the sampling action on the states. There, $\mathbf{R}(z)$ is a reference prefilter, $\mathbf{C}(z)$ a feedback controller. Once again, a single-sample processing delay is assumed [33] and represented by the block z^{-1} . The block $\mathbf{G}_h(s)$ represents the zero-order hold (ZOH), which models the action of holding the pulse width modulator register for a sampling time [34]. This block is defined by the transfer function:

$$\mathbf{G}_h(s) = \frac{1 - e^{-sT_s}}{sT_s}. \quad (1)$$

The sampling process is modelled through pulse modulation [35], in which the output signal is modulated by an infinite series of delta Dirac functions. Thus, for the case of a signal $x(t)$, the sampled output $x^*(t)$, results:

$$x^*(t) = T_s \sum_{k=0}^{\infty} x(t) \delta(t - kT_s), \quad (2)$$

where the index $*$ denotes the sampling action and δ the Dirac delta function. Applying the Laplace transform $\mathcal{L}\{\cdot\}$ to the sampled signal $x^*(t)$, we obtain

$$x^*(s) = \mathcal{L}\{x^*(t)\} = T_s \sum_{k=0}^{\infty} x(kT_s) e^{-skT_s}. \quad (3)$$

Note that the Equation (3) can be taken to an expression of the Z transform of x^* by making $z = e^{sT_s}$. On the other hand, the Equation (3) can be represented, applying the Poisson summation [36], with the form

$$x^*(s) = \sum_{k=-\infty}^{\infty} x(s + jk\omega_s), \quad (4)$$

where $\omega_s = 2\pi/T_s$ is the sampling angular frequency. The sampling operation generates harmonic components of the signal x at frequencies $k\omega_s$, with $k \in \mathbb{Z}$.

In Figure 3, the states \vec{i}_i^* , \vec{v}_c^* , \vec{i}_s^* and \vec{v}_i^* , are fed back through $\mathbf{C}_1(z)$, $\mathbf{C}_2(z)$, $\mathbf{C}_3(z)$ and $\mathbf{C}_4(z)$, respectively. There, the grid is modeled again as an impedance in series with a voltage source. The variation in this impedance causes the instability of the system.

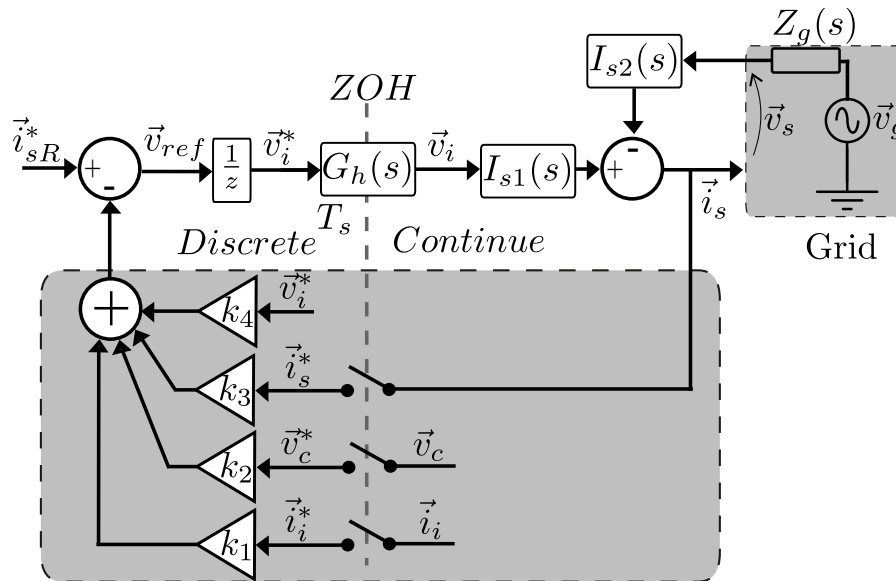


Figure 3. Schematic diagram of the controller with full state feedback.

The states \vec{i}_i , \vec{v}_c , \vec{i}_s , can be defined in terms of the voltages \vec{v}_i and \vec{v}_s , from Figure 1, as follows:

$$\vec{i}_i(s) = \mathbf{I}_{i1}(s)\vec{v}_i(s) - \mathbf{I}_{i2}(s)\vec{v}_s(s), \quad \vec{v}_c(s) = \mathbf{V}_{c1}(s)\vec{v}_i(s) - \mathbf{V}_{c2}(s)\vec{v}_s(s), \quad \vec{i}_s(s) = \mathbf{I}_{s1}(s)\vec{v}_i(s) - \mathbf{I}_{s2}(s)\vec{v}_s(s), \quad (5)$$

through the following transfer functions:

$$\begin{aligned} \mathbf{I}_{i1}(s) &= \frac{[s^2 + (b^2 - a^2)\omega_{\text{crit}}^2]}{L_T(1 - \frac{a^2}{b^2})s(s^2 + b^2\omega_{\text{crit}}^2)}, & \mathbf{I}_{i2}(s) &= -\frac{b^2\omega_{\text{crit}}^2}{L_T s(s^2 + b^2\omega_{\text{crit}}^2)}, \\ \mathbf{V}_{c1}(s) &= \frac{a^2\omega_{\text{crit}}^2}{(s^2 + b^2\omega_{\text{crit}}^2)}, & \mathbf{V}_{c2}(s) &= \frac{(b^2 - a^2)\omega_{\text{crit}}^2}{(s^2 + b^2\omega_{\text{crit}}^2)}, \\ \mathbf{I}_{s1}(s) &= \frac{b^2\omega_{\text{crit}}^2}{L_T s(s^2 + b^2\omega_{\text{crit}}^2)}, & \mathbf{I}_{s2}(s) &= -\frac{b^2(s^2 + a^2\omega_{\text{crit}}^2)}{L_T a^2 s(s^2 + b^2\omega_{\text{crit}}^2)}, \end{aligned} \quad (6)$$

with

$$b = \frac{\omega_r}{\omega_{\text{crit}}}, \quad a = \frac{\omega_{\text{ari}}}{\omega_{\text{crit}}}, \quad \omega_r = \sqrt{\frac{L_T}{L_i L_s C}}, \quad \omega_{\text{ari}} = \sqrt{\frac{1}{L_i C}}, \quad (7)$$

$L_T = L_i + L_s$, T_s the sampling time, ω_r the resonance angular frequency, ω_{ari} the anti-resonance angular frequency and $\omega_{\text{crit}} = \frac{\pi}{3T_s}$ [12]. Thus, it is possible to define all transfer functions as a function of a , b , L_T and ω_{crit} , with $b > a$.

From Figure 3, the output current \vec{i}_s can be expressed as:

$$\vec{i}_s(s) = \mathbf{I}_{s1}(s)\mathbf{G}_h(s)\vec{v}_i^*(s) - \mathbf{I}_{s2}(s)\vec{v}_s(s), \quad (8)$$

being

$$\vec{v}_i^*(s) = z^{-1}\mathbf{C}(z) \left[\vec{i}_{sR}^*(s)\mathbf{R}(z) - \mathbf{C}_1(z)\vec{i}_i^*(s) - \mathbf{C}_2(z)\vec{v}_c^*(s) - \mathbf{C}_3(z)\vec{i}_s^*(s) - \mathbf{C}_4(z)\vec{v}_i^*(s) \right]. \quad (9)$$

On the other hand, let $\mathbf{H}(s)$ be a generic transfer function in the Laplace domain, from [35] it is correct to assert:

$$[\mathbf{H}(s)\mathbf{G}_h(s)\vec{v}_i^*]^* = [\mathbf{H}(s)\mathbf{G}_h(s)]^*\vec{v}_i^* \text{ and } [\mathbf{H}(s)\mathbf{G}_h(s)]^* = \mathbf{H}(z). \quad (10)$$

Following this criterion, replacing (6) and (9) in (8), and operating, we obtain:

$$\vec{i}_s(s) = \frac{z^{-1}\mathbf{G}_h(s)\mathbf{I}_{s1}(s)\mathbf{C}(z)\mathbf{R}(z)\vec{i}_{sR}^*(s)}{\mathbf{D}(z)} - \vec{v}_s(s)\mathbf{I}_{s2}(s) + \mathbf{I}_{s1}(s)\frac{[\vec{v}_s(s)\mathbf{N}(s)]^*}{\mathbf{D}(z)}, \quad (11)$$

being

$$\mathbf{N}(s) = z^{-1}\mathbf{G}_h(s)\mathbf{C}(z) [\mathbf{I}_{i2}(s)\mathbf{C}_1(z) + \mathbf{V}_{c2}(s)\mathbf{C}_2(z) + \mathbf{I}_{s2}(s)\mathbf{C}_3(z)] \quad (12)$$

and

$$\mathbf{D}(z) = \{1 + z^{-1}\mathbf{C}(z) [\mathbf{I}_{i1}(z)\mathbf{C}_1(z) + \mathbf{V}_{c1}(z)\mathbf{C}_2(z) + \mathbf{I}_{s1}(z)\mathbf{C}_3(z) + \mathbf{C}_4(z)]\}, \quad (13)$$

where $\mathbf{I}_{i1}(z)$, $\mathbf{I}_{s1}(z)$ and $\mathbf{V}_{c1}(z)$ are the Z transforms of $\mathbf{I}_{i1}(s)$, $\mathbf{I}_{s1}(s)$ and $\mathbf{V}_{c1}(s)$, respectively, defined as follows:

$$\mathbf{I}_{i1}(z) = \frac{\Delta_i(z)}{\Delta_r(z)}, \quad \mathbf{V}_{c1}(z) = \frac{\Delta_c(z)}{\Delta_r(z)}, \quad \mathbf{I}_{s1}(z) = \frac{\Delta_s(z)}{\Delta_r(z)}, \quad (14)$$

with

$$\Delta_r(z) = (z - 1)R_r(z), R_r(z) = z^2 - 2z \cos(\phi_b) + 1, \quad (15)$$

$$\Delta_i(z) = \mathbf{C}_1(z)k_i(z^2 + b_iz + 1), \Delta_c(z) = \mathbf{C}_2(z)k_{vc}(z^2 - 1), \text{ and } \Delta_s(z) = \mathbf{C}_3(z)k_s(z^2 + b_sz + 1). \quad (16)$$

Being

$$\begin{aligned} \phi_b &= \frac{\pi b}{3}, k_i = \frac{[\frac{\pi}{3} + \gamma]}{L_T \omega_{\text{crit}}}, b_i = -2 \frac{[\frac{\pi}{3} \cos(\phi_b) + \gamma]}{[\frac{\pi}{3} + \gamma]}, \gamma = \sin(\phi_b) \frac{a^2}{b(b^2 - a^2)}, \\ k_s &= \frac{[\frac{\pi}{3} - \frac{1}{b} \sin(\phi_b)]}{L_T \omega_{\text{crit}}}, b_s = -2 \frac{[\frac{\pi}{3} \cos(\phi_b) - \frac{1}{b} \sin(\phi_b)]}{[\frac{\pi}{3} - \frac{1}{b} \sin(\phi_b)]} \text{ and } k_{vc} = \frac{a^2}{b^2} [1 - \cos(\phi_b)]. \end{aligned} \quad (17)$$

If the image terms, produced by the sampling process in (11), are neglected, it results:

$$\vec{i}_s(s) = \frac{\overbrace{z^{-1} \mathbf{G}_h(s) \mathbf{I}_{s1}(s) \mathbf{C}(z) \mathbf{R}(z) \vec{i}_{sR}^*(s)}^{\vec{i}}}{\mathbf{D}(z)} + \left[\overbrace{-\mathbf{I}_{s2}(s) + \mathbf{I}_{s1}(s) \frac{\mathbf{N}(s)}{\mathbf{D}(z)}}^{\mathbf{Y}_o(s)} \right] \vec{v}_s, \quad (18)$$

where the identity $z = e^{sT_s}$ is applied.

Operating $\mathbf{Y}_o(s)$ from (18), we obtain:

$$\mathbf{Y}_o(s) = \underbrace{\frac{b^2}{L_T s(s^2 + b^2 \omega_{\text{crit}}^2)}}_{\mathbf{\Omega}(s)} \underbrace{\left[\frac{1}{a^2} (s^2 + a^2 \omega_{\text{crit}}^2) + \omega_{\text{crit}}^2 \frac{\mathbf{N}(s)}{\mathbf{D}(z)} \right]}_{\mathbf{\Lambda}(s)}, \quad (19)$$

being

$$\mathbf{N}(s) = -\frac{3 \omega_{\text{crit}} b^2}{\pi L_T a^2} \frac{(1 - z^{-1}) n(s)}{z s^2 (s^2 + b^2 \omega_{\text{crit}}^2)}, \quad (20)$$

with

$$n(s) = \mathbf{C}(z) \left\{ \mathbf{C}_3(s) s^2 - \mathbf{C}_2(s) L_T a^2 \left(1 - \frac{a^2}{b^2} \right) \omega_{\text{crit}}^2 s + a^2 \omega_{\text{crit}}^2 [\mathbf{C}_1(z) + \mathbf{C}_3(z)] \right\} \quad (21)$$

and

$$\mathbf{D}(z) = \frac{d(z)}{z \Delta_r(z)}, \quad (22)$$

being

$$d(z) = [z + \mathbf{C}_4(z)] \Delta_r(z) + \Delta_i(z) + \Delta_s(z) + \Delta_c(z). \quad (23)$$

Replacing, and operating, it results:

$$\Lambda_2(s) = \frac{\overbrace{(z-1)^2}^{\Phi_1(s)}}{z s^2} \frac{3 \omega_{crit}^3 b^2}{\pi L_T a^2} \underbrace{\frac{R_r(z)}{z(s^2 + b^2 \omega_{crit}^2)}}_{\Phi_2(s)} \underbrace{\frac{(-z) n(s)}{d(z)}}_{\Phi_3(s)} \quad (24)$$

It is important to note that $\Phi_1(s)$ and $\Phi_2(s)$ have zero phase for all frequency values, so the phase of $\Lambda_2(s)$ will be given by $\Phi_3(s)$, and therefore, by the phase difference between $-n(s)$ and $\frac{d(z)}{z}$.

For the system stability analysis, the disturbance signal $\vec{v}_g = 0$ is considered, since it does not affect the system stability. From Figure 2, it is straightforward to calculate the output current as follows:

$$\vec{i}_s = \frac{1}{1 + \mathbf{Y}_o(s)Z_g(s)} \vec{I} \quad (25)$$

To ensure the stability of the system it is necessary that the denominator of (25) satisfies the Nyquist criterion. Therefore, for the design of a robust controller for any value of L_g and R_g , the phase of the product $\mathbf{Y}_o(s)Z_g(s)$ must not cross the negative real axis. In addition, it must be satisfied that \vec{I} possesses poles [zeros of $d(z)$] inside the unit circle.

For the limiting cases where the impedance $Z_g(s)$ is a resistance or an inductance, it would contribute respectively a phase of 0° or 90° to the phase of the product $\mathbf{Y}_o(s)Z_g(s)$. It follows that for the system to be robust to variations in the grid impedance, $-180^\circ < \angle \mathbf{Y}_o(s) < 90^\circ$, as shown in Figure 4. The difficulty lies in finding the values of $\mathbf{C}(z)$, $\mathbf{C}_1(z)$, $\mathbf{C}_2(z)$, $\mathbf{C}_3(z)$ and $\mathbf{C}_4(z)$, which allow the transfer function $\mathbf{Y}_o(s)$ (18) to satisfy the phase requirement that guarantees stability in the presence of an unknown grid impedance.

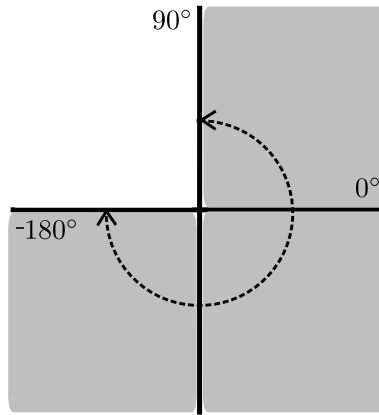


Figure 4. Phase values allowed for $\mathbf{Y}_o(s)$.

From Equation (19), it is evident that $\Omega(s)$ exhibits a phase of -90° for $\omega < b\omega_{crit}$, and 90° for $\omega > b\omega_{crit}$. Consequently, for the scenario where $\omega < b\omega_{crit}$, $-90^\circ < \angle \Lambda(s) < 180^\circ$ must be ensured. Likewise, for $\omega \geq b\omega_{crit}$, it is necessary that $90^\circ < \angle \Lambda(s) < 360^\circ$, to satisfy the Nyquist criterion detailed in Equation (25).

Additionally, it is evident from Equation (19) that the gains of feedback dominating the phase behavior of $\mathbf{Y}_o(s)$ are contained within $\Lambda_2(s)$, specifically within $\Phi_3(s)$. Moreover, note that $s \rightarrow 0$: $\mathbf{Y}_o(s)$ approaches $\left[\frac{1 + \mathbf{C}_2(z) + \mathbf{C}_4(z)}{\mathbf{C}_1(z) + \mathbf{C}_3(z)} \right]_{|z=1}$.

On the other hand, to ensure the closed-loop stability of the system, the zeros of $d(z)$ must be inside the unit circle. For this, it is necessary to ensure that the open-loop response of the system does not cross 180° with modulus greater than

or equal to one. Considering the schematic depicted in Figure 3, the open-loop response, for the case where the current loop \vec{i}_s is opened, results:

$$\mathbf{O}_L(z) = \frac{\Delta_s}{[z + \mathbf{C}_4(z)]\Delta_r(z) + \Delta_i(z) + \Delta_c(z)}, \quad (26)$$

where $\mathbf{O}_L(z)$ is the open-loop transfer function.

The following section will detail the behaviour of the output admittance and the open-loop response of the system, for the case where different states are fed back. In the following, the parameter values defined in Table 1 will be used for the output admittance analysis.

Table 1. Parameters

Parameters	Values
L_T	3.78 mH
f_s	9 kHz
ω_{crit}	2π 1.5 kHz

4. System analysis for different feedback types

In this section, the stability of the system will be studied for different types of feedback, determining the stability limits of each one. Then, a criterion of gain choices will be proposed to ensure the stability of the system for any R-L type impedance values. Ensuring that the closed-loop poles are in positions that guarantee stability, for any value of grid inductance, and that the Nyquist stability criterion is satisfied. For this, the transfer functions of the controller will be defined as gains, being $\mathbf{C}(z) = 1$, $\mathbf{C}_1(z) = k_1$, $\mathbf{C}_2(z) = k_2$, $\mathbf{C}_3(z) = k_3$ and $\mathbf{C}_4(z) = k_4$.

4.1 Inverter-side current feedback system analysis

In this section, the behaviour of the output admittance where only \vec{i}_i^* is fed back through the gain k_1 , while k_2 , k_3 , and k_4 are set to zero is analysed. When the value of b (7) is less than 1, it becomes feasible to achieve stable positions for all the closed-loop poles of the system by feeding back only \vec{i}_i^* through the gain k_1 [14, 37].

Furthermore, by considering Equations (21) and (23), it follows that $n(s) = a^2 \omega_{\text{crit}}^2 k_1$ and $d(z) = z\Delta_r(z) + \Delta_i(z)$. Consequently, the expression for the $\Phi_3(s)$ term in Equation (24) can be determined as follows:

$$\Phi_3(s) = \frac{(-1)n(s)}{\frac{d(z)}{z}} = \frac{(-1)(a^2 \omega_{\text{crit}}^2 k_1)}{\Delta_r(z) + \frac{\Delta_i(z)}{z}}. \quad (27)$$

In this scenario, $\Phi_3(s)$ is influenced by $\Delta_r(z) + \frac{\Delta_i(z)}{z}$. Figure 5 presents the frequency response of $\Delta_r(z)$ (15) for different values of b . It is evident that when $b < 1$, $\Delta_r(z)$ avoids crossing the 180° phase boundary. At $b = 1$, $\Delta_r(z)$ has a phase of 180° at $\omega = \omega_{\text{crit}}$. Moreover, for values of $b > 1$, $\Delta_r(z)$ crosses the 180° phase point at both $\omega = \omega_{\text{crit}}$ and $\omega = b\omega_{\text{crit}}$.

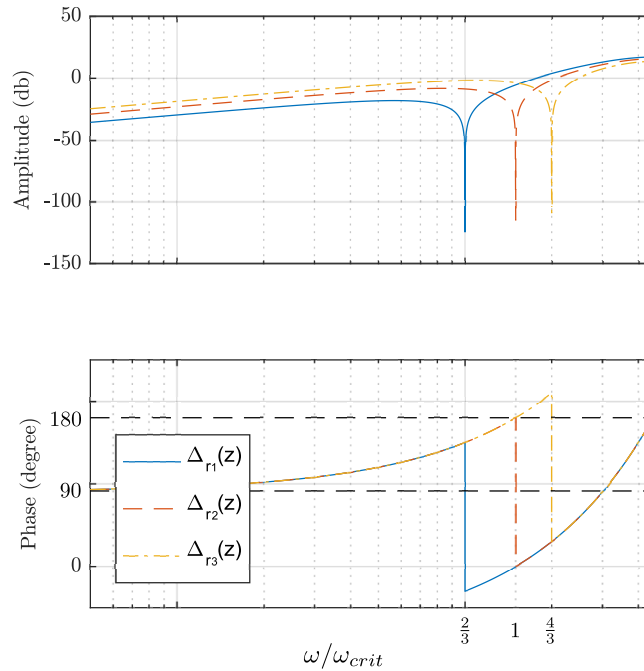


Figure 5. Frequency response of $\Delta_r(z)$ for different values of b . $\Delta_{r1}(z)$ corresponds to $b = \frac{2}{3}$, $\Delta_{r2}(z)$ corresponds to $b = 1$ and $\Delta_{r3}(z)$ corresponds to $b = \frac{4}{3}$.

Furthermore, the quotient $\frac{\Delta_i(z)}{z}$ can be expressed as a function of ω , such that $\frac{\Delta_i}{z}(\omega) = k_1 k_i [2 \cos(\omega T_s) + b_i]$. This function exclusively assumes real values and has a phase shift from 0° to 180° for $\omega \leq b\omega_{crit}$, with the frequency of the phase shift depending of the value of b_i (16).

Additionally, in coherence with the preceding section, it is crucial to verify that $-90^\circ < \angle \mathbf{\Lambda}(s) < 180^\circ$ remains valid for $\omega < b\omega_{crit}$ and $90^\circ < \angle \mathbf{\Lambda}(s) < 360^\circ$ for $\omega \geq b\omega_{crit}$ to fulfill the Nyquist stability criterion for the product of $\mathbf{Y}_o(s)$ and $\mathbf{Z}_g(s)$.

For values of $b < 1$, the phase of $\frac{d(z)}{z}$ remains constrained within the range between -90° and 180° . Consequently, the phase of $\mathbf{\Lambda}(s)$ also follows the condition $-90^\circ < \angle \mathbf{\Lambda}(s) < 180^\circ$ for $\omega < b\omega_{crit}$. This ensures that the phase requirement for $\mathbf{Y}_o(s)$ is satisfied.

On the other hand, for values of $b \geq 1$ and within the range $\omega_{crit} < \omega < b\omega_{crit}$, $\frac{d(z)}{z}$ assumes phase values between -180° and 0° . Consequently, $\mathbf{\Lambda}_2(s)$ has a phase greater than 180° within this frequency range. As a result, $\mathbf{Y}_o(s)$ exceeds 90° , and the phase requirement is not satisfied.

Hence, when only \vec{i}_i is fed back, the Nyquist criterion is satisfied in Equation (25) exclusively for values of b that are less than 1.

Furthermore, considering the situation where only \vec{i}_i is fed back and the current loop \vec{i}_i^* remains open, the open-loop response of the system can be expressed as follows:

$$\mathbf{O}_{L_i}(z) = \frac{\Delta_i(z)}{z\Delta_r}. \quad (28)$$

The open-loop transfer function $\mathbf{O}_{L_i}(z)$ crosses the 180° at $\omega = \omega_{crit}$. Therefore, if $\mathbf{O}_{L_i}(z) |_{\omega=\omega_{crit}}$ is equal to -1 , we derive:

$$k_{1crit} = \frac{L_T \omega_{crit} [1 - 2 \cos(\phi_b)]}{\frac{\pi}{3} [1 - 2 \cos(\phi_b)] - \gamma}. \quad (29)$$

Here, $k_{1\text{crit}}$ represents the value of k_1 at which a pair of closed-loop poles reside on the unit circle. To guarantee stable positions for the closed-loop poles of the system, it is essential for k_1 to be set at values lower than $k_{1\text{crit}}$.

Additionally, when considering a non-zero grid inductance L_g , the open-loop response of the system $\mathbf{O}_L(z)$ changes, causing a shift in the resonance of the LCL filter. This resonance value becomes

$$\omega_{rg} = \sqrt{\frac{L_{Tg}}{L_i(L_s + L_g)C}} = b_g \omega_{\text{crit}}, \quad (30)$$

where $L_{Tg} = L_i + L_s + L_g$. As a consequence, the value of $k_{1\text{crit}}$ (29) changes with varying L_g . In the scenario where $L_g \rightarrow \infty$, $b_g \rightarrow a$, and $k_{1\text{crit}} \rightarrow k_{1\text{critmax}}$, with

$$k_{1\text{critmax}} = \frac{(-1)L_T \left(1 - \frac{a^2}{b^2}\right) \omega_{\text{crit}} a [1 - 2\cos(\phi_a)]}{\sin(\phi_a)}, \quad (31)$$

being $\phi_a = a\frac{\pi}{3}$. Thus, as $k_{1\text{critmax}}$ increases with larger L_g , it is feasible to guarantee closed-loop pole stability by selecting a gain value $k_1 < k_{1\text{crit}}$ for $L_g = 0$ and $b < 1$.

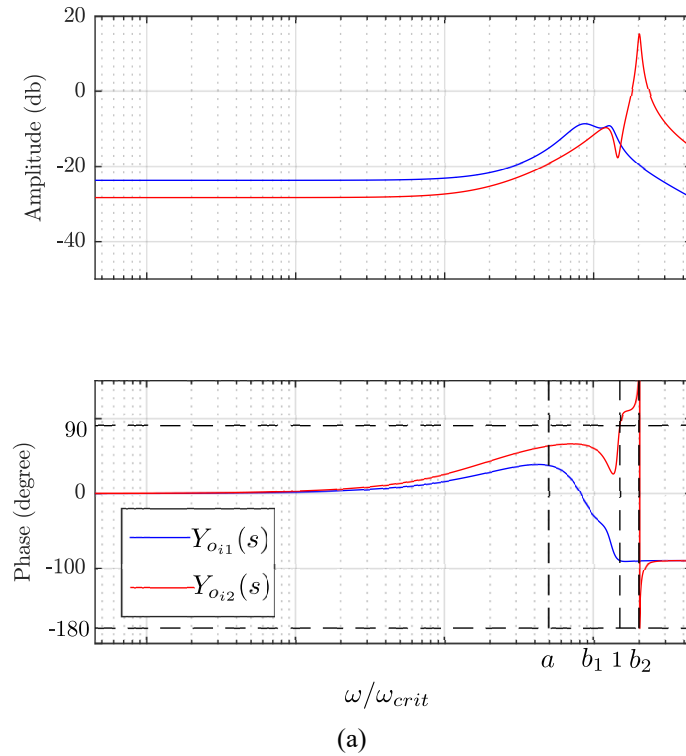


Figure 6. Cont.

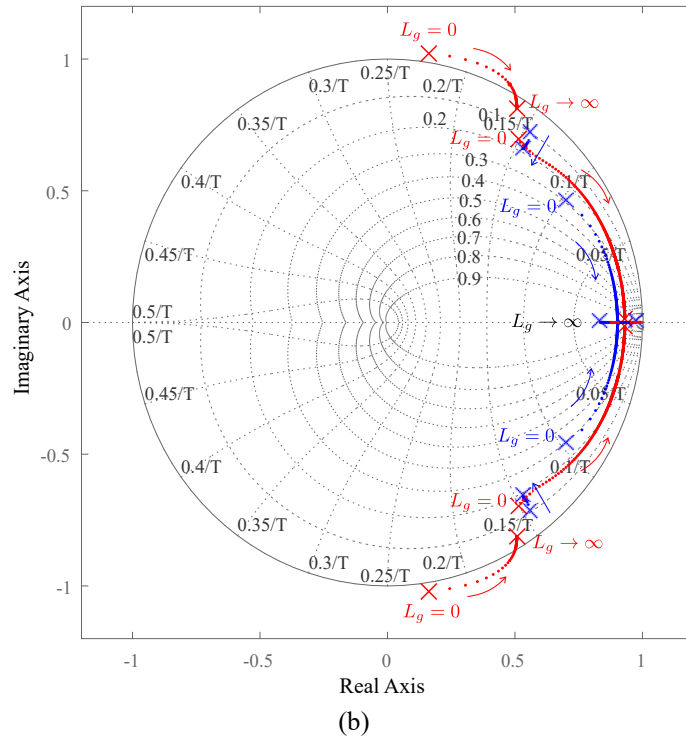


Figure 6. (a) Output admittances $\mathbf{Y}_o(s)$ for the case in which \vec{i}_i is fed back. The admittance $\mathbf{Y}_{o1}(s)$ represents the case in which $b = b_1 = \frac{2}{3}$. The admittance $\mathbf{Y}_{o2}(s)$ represents the case in which $b = b_2 = \frac{4}{3}$. (b) Location of the closed-loop poles when \vec{i}_i is fed back, for $b = b_1 = \frac{2}{3}$ (red) and $b = b_2 = \frac{4}{3}$ (blue)

In Figure 6a, the output admittance is depicted for the case where \vec{i}_i is fed back, with values of $b = b_1 = \frac{2}{3}$, $b = b_2 = \frac{4}{3}$, and $a = \frac{1}{3}$. Here, $k_1 = \frac{k_{1\text{crit}}}{\sqrt{2}}$ (29) was considered. For the $\mathbf{Y}_{o1}(s)$ case, with $b = b_1 = \frac{2}{3}$, the output admittance satisfies the phase requirement, and the Nyquist stability criterion in (25). Conversely, considering $\mathbf{Y}_{o2}(s)$ with $b = b_2 = \frac{4}{3}$, the output admittance does not satisfy the phase requirement within the $\omega_{\text{crit}} \leq \omega < b\omega_{\text{crit}}$ frequency range.

Moreover, Figure 6b illustrates the positions of the closed-loop [zeros of $d(z)$] poles when only \vec{i}_i is fed back, being $k_1 = \frac{k_{1\text{crit}}}{\sqrt{2}}$. The cases considered involve $a = \frac{1}{3}$ for $b = b_1 = \frac{2}{3}$ (shown in blue) and $b = b_2 = \frac{4}{3}$ (shown in red), varying L_g . In the case of $b = b_1 = \frac{2}{3}$, the poles reside within the unit circle. However, in the scenario of $b = b_2 = \frac{4}{3}$, there are poles located outside the unit circle as expected.

Based on the preceding analysis, it can be concluded that when $b < 1$ and \vec{i}_i is fed back, the product between the output admittance $\mathbf{Y}_o(s)$ and $Z_g(s)$ satisfy the Nyquist criterion and the closed-loop poles are positioned in stable locations. Conversely, for values of $b \geq 1$, ensuring the stability of the system becomes unattainable.

4.2 Grid-side current feedback system analysis

In this section, the scenario in which \vec{i}_s^* is fed back through the gain k_3 , with k_1 , k_2 , and k_4 set to zero, is analysed. In this specific case, the closed-loop poles of the system will invariably exist outside or on the unit circle for values of $b \leq 1$ (7). However, for values of b greater than 1, it becomes feasible to position the closed-loop poles in stable locations [12].

In this case, by utilizing (21) and (23), we deduce that $n(s) = k_3(s^2 + a^2\omega_{\text{crit}}^2)$ and $d(z) = z\Delta_r(z) + \Delta_x$. Consequently, the expression for $\Phi_3(s)$ (27) can be formulated as follows:

$$\Phi_3 = \frac{-n(s)}{\frac{d(z)}{z}} = \frac{(-1)k_3(s^2 + a^2\omega_{\text{crit}}^2)}{\Delta_r(z) + \frac{\Delta_x}{z}} \quad (32)$$

Observe in (32) that it contains the same zero as $\Lambda_1(s)$ (19). Thus, it becomes possible to rearrange $\Lambda(s)$ as follows:

$$\Lambda(s) = \Lambda_1(s) [1 + \Lambda_2'(s)], \quad (33)$$

where $\Lambda_2'(s) = \frac{\Lambda_2(s)}{\Lambda_1(s)}$.

On the other hand, it is feasible to express the ratio $\frac{\Delta_s(z)}{z}$ as a function of ω , denoted as $\frac{\Delta_s}{z}(\omega) = k_3 k_s [2 \cos(\omega T_s) + b_s]$. This function takes real and positive values (with a phase of zero) within the frequency range that is being analysed.

In Figure 5, it is evident that in situations where $\omega < \omega_{\text{crit}}$ and $\omega < b\omega_{\text{crit}}$, $\frac{\Delta_r(z)}{z}$ remains confined to phase values ranging from 90° to 180° . Furthermore, given the zero phase of $\frac{\Delta_s}{z}$, the phase of $\frac{\Delta(z)}{z}$ will be constrained within the phase interval of 0° to 180° . Consequently, $\Lambda_2'(s)$ will exhibit a phase greater than 0° and less than 180° for $\omega < \omega_{\text{crit}}$. The same principle applies to the $(1 + \Lambda_2'(s))$ term in (33), which will also be confined to this phase range for $\omega < \omega_{\text{crit}}$.

In cases where $a < 1$ (7), $\Lambda_1(s)$ crosses the 180° boundary for $\omega < \omega_{\text{crit}}$. Consequently, the phase of $\Lambda(s)$ takes values between -180° and -90° within the range of $a\omega_{\text{crit}} < \omega \leq \omega_{\text{crit}}$. This results in $\mathbf{Y}_o(s)$ assuming a phase greater than 90° , which means it does not satisfy the phase requirement. Conversely, in the scenario where $a = 1$, $\mathbf{Y}_o(s)$ holds a phase of 90° exclusively at $\omega = \omega_{\text{crit}}$.

In cases where $a > 1$, it is possible to get $\mathbf{Y}_o(s)$ satisfies the phase requirement. To achieve this, it is imperative that $\frac{\Delta(z)}{z}$ avoids taking values between -180° and -90° for $\omega < b\omega_{\text{crit}}$. Referring to (33), it becomes necessary that $\Re\{\Lambda_2'(s)\}$ exceeds -1 within the range of $\omega_{\text{crit}} \leq \omega \leq a\omega_{\text{crit}}$. This objective can be accomplished by ensuring that k_3 remains below a critical threshold value, denoted as $k_{3\text{crit}}$, at which $\Re\{\Lambda_2'(s)\} = -1$ for the frequency $\omega = a\omega_{\text{crit}}$.

On the other hand, from (26), the open-loop response for the case where only \vec{i}_s is fed back results in $\mathbf{O}_{Ls}(z) = \frac{\Delta_s}{z\Delta_r}$. $\mathbf{O}_{Ls}(z)$ only crosses the 180° phase at $\omega = \omega_{\text{crit}}$ and $\omega = b\omega_{\text{crit}}$. Once again, by evaluating the open-loop response at $\omega = \omega_{\text{crit}}$, equalling to -1 , and resolving, results:

$$k_{3\text{crit}} = \frac{L_T \omega_{\text{crit}} [1 - 2 \cos(\phi_b)]}{\frac{\pi}{3} [1 - 2 \cos(\phi_b)] + \frac{\sin(\phi_b)}{b}}, \quad (34)$$

where $k_{3\text{crit}}$ is the critical gain value for which the closed-loop poles are located on the unit circle. Hence, to position the closed-loop poles in stable positions, it is imperative that k_3 remains below $k_{3\text{crit}}$. As the open-loop response changes with variations in L_g , the value of $k_{3\text{crit}}$ also changes, decreasing as L_g increases. In the scenario where $L_g \rightarrow \infty$, $b_g \rightarrow a$ (30) and $k_{3\text{crit}} \rightarrow k_{3\text{crit}_{\text{min}}}$, being:

$$k_{3\text{crit}_{\text{max}}} = \frac{L_T \omega_{\text{crit}} [1 - 2 \cos(\phi_a)]}{\frac{\pi}{3} [1 - 2 \cos(\phi_a)] + \frac{\sin(\phi_a)}{a}}. \quad (35)$$

Therefore, to ensure that the closed-loop poles are located in stable positions for any value of L_g and $b_g > 1$, it is necessary to satisfy the condition $k_3 < k_{3\text{crit}_{\text{min}}}$.

Figure 7a shows the output admittances $\mathbf{Y}_{o_{s1}}(s)$ and $\mathbf{Y}_{o_{s2}}(s)$ corresponding to $a = a_1 = \frac{4}{3}$ and $a = a_2 = \frac{2}{3}$, respectively, being $b = \frac{5}{3}$ and $k_3 = \frac{1}{\sqrt{2}} k_{3\text{crit}_{\text{min}}}$ for $a = a_1$. Notably, for $\mathbf{Y}_{o_{s2}}(s)$, within the frequency range of $a\omega_{\text{crit}} < \omega < \omega_{\text{crit}}$, the phase exceeds 90° , thereby not satisfying the phase requirement. Conversely, for the case of $\mathbf{Y}_{o_{s1}}(s)$, the phase remains confined within the permissible limits, thereby satisfying the Nyquist stability criterion.

In Figure 7b, the placements of the closed-loop poles are illustrated while varying L_g for the previously discussed case. Notably, for the instance where $a = a_1 = \frac{4}{3}$ (depicted in red), as $L_g \rightarrow \infty$, $b_g \rightarrow a_1$ (30), consequently maintaining the closed-loop poles within the unit circle. Conversely, in the case of $a = a_2 = \frac{2}{3}$ (shown in blue), as $L_g \rightarrow \infty$, $b_g \rightarrow a_2$, there are some closed-loop poles located outside the unit circle.

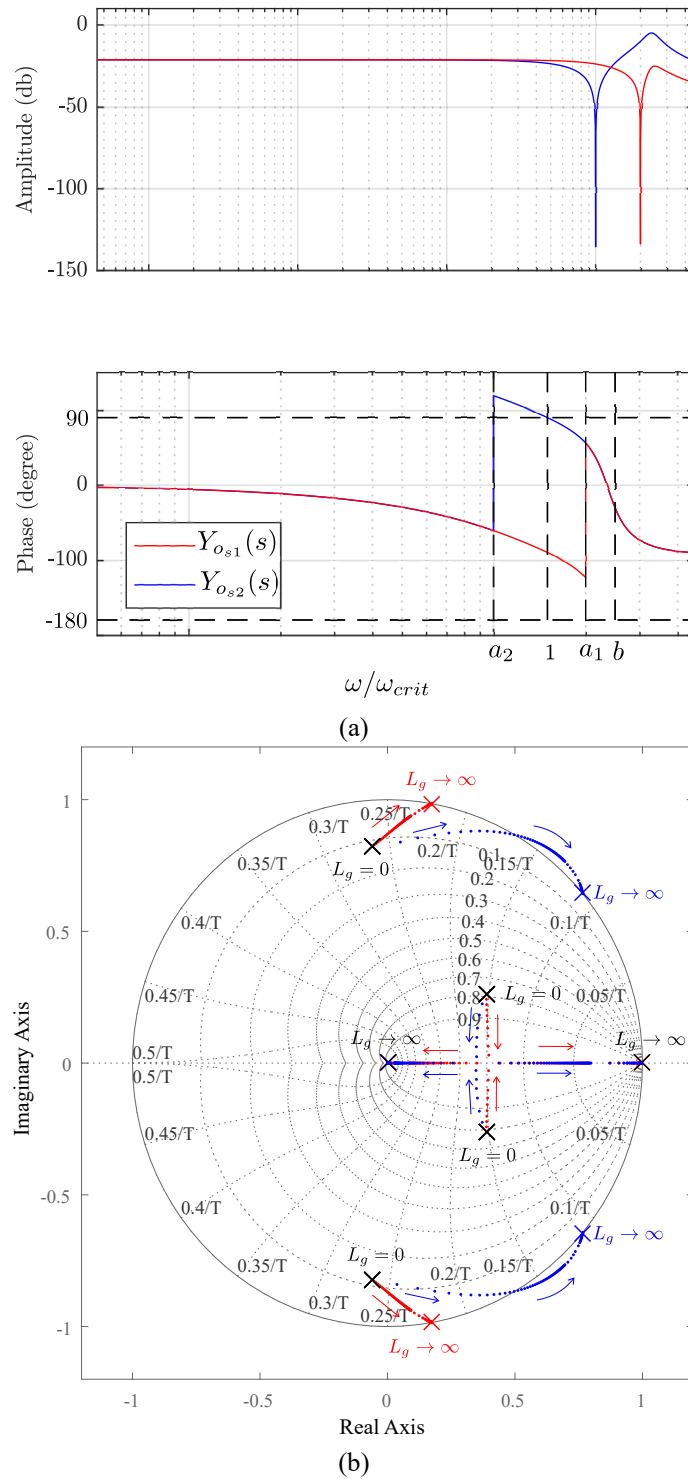


Figure 7. (a) Output admittances $\mathbf{Y}_o(s)$ for the case in which \vec{i}_s is fed back. The admittance $\mathbf{Y}_{o_{s1}}(s)$ represents the case in which $a = a_1 = \frac{4}{3}$. The admittance $\mathbf{Y}_{o_{s2}}(s)$ represents the case in which $a = a_2 = \frac{2}{3}$. (b) Location of the closed-loop poles when \vec{i}_s is fed back, for $a = a_1 = \frac{4}{3}$ (blue) and $a = a_2 = \frac{2}{3}$ (red)

In summary, in cases where \vec{i}_s is fed back and $a > 1$, it becomes feasible for the the product between $\mathbf{Y}_o(s)$ and $Z_g(s)$ to satisfy the Nyquist criterion and position the closed-loop poles in stable locations even when subjected to variations in L_g .

However, when $a \leq 1$, despite the closed-loop poles potentially being stable (for $b_g > 1$), it is unachievable to guarantee that $\mathbf{Y}_o(s)$ complies with the phase requirement.

4.3 Currents feedback system analysis

In this section, we will analyse the scenario where both \vec{i}_i^* and \vec{i}_s^* are fed back through the gains k_1 and k_3 , respectively, while considering k_2 and k_4 as zero, for the case where $a < 1$ and $b \geq 1$ (7).

For this case, based on (21) and (23), results $n(s) = [k_3 s^2 + a^2 \omega_{crit}^2 (k_1 + k_3)]$ and $d(z) = z\Delta_r(z) + \Delta_i + \Delta_s$. Moreover, if the gains k_1 and k_3 are defined as follows:

$$k_1 = \lambda \omega_{crit} L_T (\lambda_1^2 - a^2) \text{ and } k_3 = \lambda \omega_{crit} L_T a^2, \quad (36)$$

results $n(s) = \lambda \omega_{crit} L_T a^2 [s^2 + \lambda_1^2 \omega_{crit}^2]$, where λ and λ_1 are gains to be defined.

For values of $1 < \lambda_1 < b$, within the frequency range $\omega < \omega_{crit}$, $\frac{\vec{z}}{d(\vec{z})}$ exhibits a phase between 0° and 180° . Consequently, it is possible to achieve that, for $\omega < \omega_{crit}$ and $1 < \lambda_1 < b$, $0^\circ < \angle \mathbf{\Lambda}(s) < 180^\circ$, ensuring that $\mathbf{Y}_o(s)$ satisfies the phase requirement.

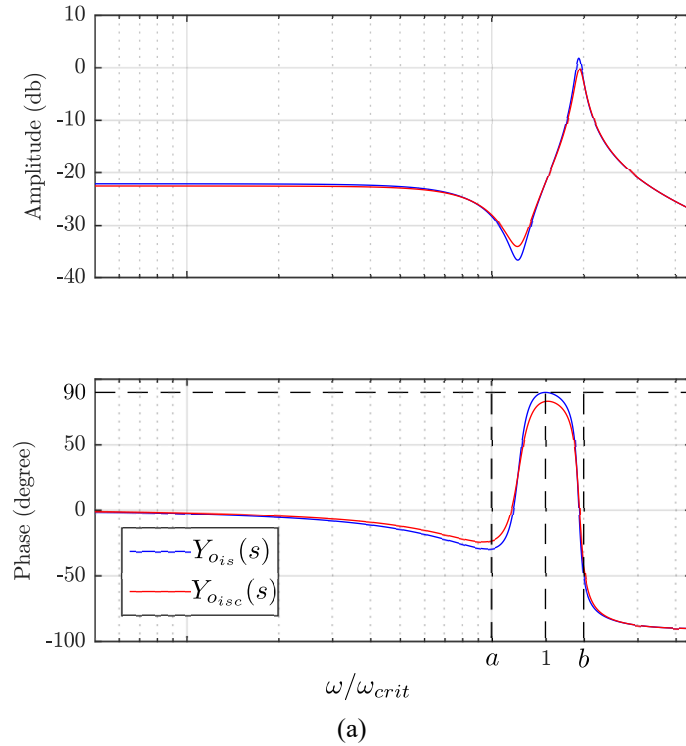


Figure 8. Cont.

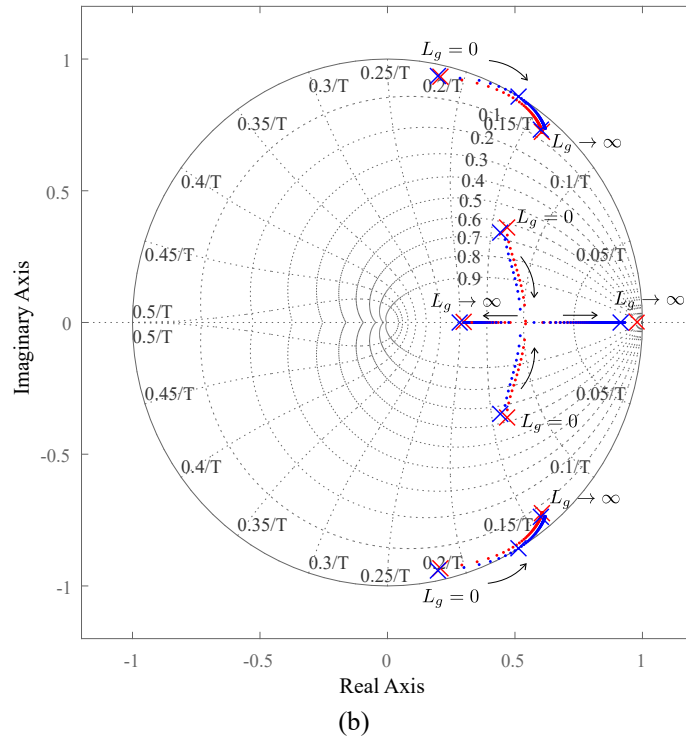


Figure 8. (a) Output admittance $\mathbf{Y}_{ois}(s)$ for the case when the currents \vec{i}_i and \vec{i}_s are fed back. Output admittance $\mathbf{Y}_{oisc}(s)$ for the case in which the states \vec{i}_i , \vec{v}_c and \vec{i}_s are fed back. (b) Location of the closed-loop poles for the case in which the currents \vec{i}_i and \vec{i}_s are fed back (blue) and in which \vec{i}_i , \vec{v}_c and \vec{i}_s are fed back (red)

In the frequency range $\omega_{crit} \leq \omega \leq \lambda_1 \omega_{crit}$, for $1 \leq \lambda_1 \leq b$, the feedback of \vec{i}_i and \vec{i}_s currents does not guarantee that $\mathbf{Y}_o(s)$ satisfy the phase requirement. This is due to for values between $\omega_{crit} \leq \omega \leq b\omega_{crit}$, $\frac{-z}{d(z)}$ takes phase values less than zero. This produces that for $\omega_{crit} \leq \omega \leq \lambda_1 \omega_{crit}$, $-180^\circ < \angle \mathbf{\Lambda}(s) - 90^\circ$ and $\angle \mathbf{Y}_o(s) > 90^\circ$. On the other hand, for the case where $\lambda_1 = 1$, the only point of $\angle \mathbf{Y}_o(s) = 90^\circ$ is at $\omega = \omega_{crit}$.

Furthermore, for $\omega > b\omega_{crit}$, $180^\circ < \angle \mathbf{\Lambda}(s) < 0^\circ$, thus $\mathbf{Y}_o(s)$ satisfies the phase requirement for this frequency range.

Indeed, when dealing with the scenario where $a < 1$ and $b \geq 1$, it is not feasible to satisfy the Nyquist stability criterion by fed back \vec{i}_i and \vec{i}_s . In the particular case where $\lambda_1 = 1$, $\angle \mathbf{Y}_o(s) = 90^\circ$ at $\omega = \omega_{crit}$.

On the other hand, to determine the closed-loop stability of the system, the open-loop response $\mathbf{O}_L(z)$ (26), is analysed. When exclusively \vec{i}_i and \vec{i}_s are fed back, the frequencies at which the open-loop response crosses the 180° phase are $\omega = \omega_{crit}$ and $\omega = b\omega_{crit}$. Consequently, upon assessing the open-loop response at these frequencies, we obtain:

$$O_{L\omega_{crit}} = \frac{num\{O_{L\omega_{crit}}\}}{den\{O_{L\omega_{crit}}\}}, \quad (37)$$

$$num\{O_{L\omega_{crit}}\} = \lambda a^2 \left\{ \frac{\pi}{3} [1 - 2 \cos(\phi_b)] + \frac{1}{b} \sin(\phi_b) \right\}, \quad (38)$$

$$den\{O_{L\omega_{crit}}\} = (-1) [1 - 2 \cos(\phi_b)] + \lambda (\lambda_1^2 - a^2) \left[\frac{\pi}{3} [1 - 2 \cos(\phi_b)] - \gamma \right],$$

$$O_{Lb\omega_{crit}} = \frac{(b^2 - a^2)}{(-1)(\lambda_1^2 - a^2)}, \quad (39)$$

where $O_{L\omega_{\text{crit}}}$ and $O_{Lb\omega_{\text{crit}}}$ represent the open-loop frequency response at $\omega = \omega_{\text{crit}}$ and $\omega = b\omega_{\text{crit}}$, respectively. In the specific instance where $b = \lambda_1 = 1$, the open-loop response $O_{Lb\omega_{\text{crit}}}$ equates to -1 , indicating the presence of a pair of closed-loop poles [zeros of $d(z)$] situated above the unit circle.

For the scenario where $O_{L\omega_{\text{crit}}} = -1$ and operating in (37), results:

$$\lambda_{\text{crit}} = \left(1 - \frac{a^2}{b^2}\right) \psi, \quad (40)$$

being

$$\psi = \left\{ \sin(\phi_b) \frac{a^2}{b} \frac{\left(1 - \frac{\lambda_1^2}{b^2}\right)}{[1 - 2\cos(\phi_b)]} + \lambda_1^2 \frac{\pi}{3} \left(1 - \frac{a^2}{b^2}\right) \right\}^{-1}. \quad (41)$$

where λ_{crit} represents the value of λ at which the open-loop response intersects the 180° phase line with a modulus of one at $\omega = \omega_{\text{crit}}$. Hence, in order to guarantee that the closed-loop poles remain inside the unit circle, it is imperative that $\lambda < \lambda_{\text{crit}}$. Given that ψ is consistently greater than $\frac{3}{\pi}$, λ can be defined as:

$$\lambda = \varepsilon \frac{3}{\pi} \left(1 - \frac{a^2}{b^2}\right). \quad (42)$$

For $\varepsilon < 1$, λ will consistently remain less than λ_{crit} . This ensures that the open-loop response will never cross the 180° phase line with a modulus greater than one at $\omega = \omega_{\text{crit}}$, except when $b = 1$.

Additionally, changes in L_g lead to variations in $\mathbf{O}_L(z)$ and λ_{crit} . In the particular scenario where $L_g \rightarrow \infty$, $b_g \rightarrow a$ (30), and $\lambda_{\text{crit}} \rightarrow \lambda_{\text{crit}_{\text{min}}}$, where

$$\lambda_{\text{crit}_{\text{min}}} = \frac{[1 - 2\cos(\phi_a)] a}{\sin(\phi_a)(a^2 - \lambda_1^2)} \left(1 - \frac{a^2}{b^2}\right), \quad (43)$$

the minimum value that λ_{crit} could attain. Therefore, it is possible to ensure that the closed-loop poles are in stable positions for variations in L_g by choosing a value of λ_{crit} that is less than $\lambda_{\text{crit}_{\text{min}}}$, except for the case where $b_g = 1$, which results in a pair of poles on the unit circle.

In Figure 8a, the output admittance is shown. There, $\mathbf{Y}_{o_{is}}(\mathbf{s})$ represents the value of the output admittance for $a = \frac{2}{3}$, $b = \frac{4}{3}$, $\varepsilon = \frac{1}{2}$, and $\lambda_1 = 1$, when \vec{i}_i and \vec{i}_s are fed back. It can be observed that the output admittance $\mathbf{Y}_{o_{is}}(s)$ satisfies the phase requirement for all frequency values except at ω_{crit} , where the output admittance phase is 90° .

In Figure 8b, the location of the closed-loop poles of the system is depicted by varying L_g , with \vec{i}_i and \vec{i}_s fed back (shown in blue). The parameters used are $a = \frac{2}{3}$, $b = \frac{4}{3}$, $\varepsilon = \frac{1}{2}$, and $\lambda_1 = 1$. It can be observed that all the poles are positioned within the unit circle, except for the case where $b_g = 1$, leading to a pair of poles on the unit circle.

Absolutely, despite the potential to achieve stable locations for closed-loop poles in cases where $b_g \neq 1$, it remains impossible for $\mathbf{Y}_o(s)$ to fulfil the phase requirement at $\omega = \omega_{\text{crit}}$. To overcome these challenges concerning both closed-loop pole stability and the phase characteristic of $\mathbf{Y}_o(s)$, the following section includes the fed back of \vec{v}_c^* and \vec{v}_i^* through k_2 and k_4 gains, respectively.

4.4 Full state feedback system analysis.

In this section, we will analyse the scenario in which the state variables \vec{i}_i^* , \vec{v}_c^* , \vec{i}_s^* , and \vec{v}_i^* are fed back using the gains k_1 , k_2 , k_3 , and k_4 respectively.

For the defined gain values in (36), $k_2 = \lambda \lambda_2$ and currently $k_4 = 0$, results:

$$n(s) = \lambda \omega_{\text{crit}} L_T a^2 \left[s^2 - \lambda_2 \left(1 - \frac{a^2}{b^2} \right) \omega_{\text{crit}} s + \lambda_1 \omega_{\text{crit}}^2 \right], \quad (44)$$

and $d(z) = z\Delta_r(z) + \Delta_i(z) + \Delta_s(z) + \Delta_c(z)$ (23), being λ_2 a gain to be defined. Indeed, when \vec{v}_c is fed back, it results in $n(s)$ having a phase equal to $\pm 90^\circ$ for the case of $\lambda_1 = 1$ and at $\omega = \omega_{\text{crit}}$. Additionally, the phase of $\frac{\Delta_c(z)}{z}$ (16) becomes $\pm 90^\circ$, with both signs determined by the value of k_2 .

Certainly, the open-loop response $O_L(z)$ evaluated at $\omega = \omega_{\text{crit}}$ and $\omega = b\omega_{\text{crit}}$ is given by the following expressions:

$$O_{L\omega_{\text{crit}}} = \frac{\text{num}\{O_{L\omega_{\text{crit}}}\}}{\text{den}\{O_{L\omega_{\text{crit}}}\}}, \quad (45)$$

being

$$\text{num}\{O_{L\omega_{\text{crit}}}\} = \lambda a^2 \left\{ \pi/3 [1 - 2 \cos(\phi_b)] + \frac{1}{b} \sin(\phi_b) \right\}, \quad (46)$$

$$\text{den}\{O_{L\omega_{\text{crit}}}\} = (-1)[1 - 2 \cos(\phi_b)] + \lambda (\lambda_1^2 - a^2) \left[\frac{\pi}{3} [1 - 2 \cos(\phi_b)] - \gamma \right] + j\sqrt{3}\lambda \lambda_2 \frac{a^2}{b^2} [1 - \cos(\phi_b)],$$

and

$$O_{Lb\omega_{\text{crit}}} = \frac{(b^2 - a^2)}{(-1)(\lambda_1^2 - a^2) + j\frac{\lambda_2}{b}(b^2 - a^2)}. \quad (47)$$

Thus, with the correct choice of λ_2 , it is possible to achieve that O_L crosses the 180° with modulus less than one, similar to what was developed in [17].

On the other hand, if $\lambda_2 = -\rho \left(1 - \frac{a^2}{b^2} \right)^{-1}$, results $n(s) = \lambda \omega_{\text{crit}} L_T a^2 [s^2 + \rho \omega_{\text{crit}} s + \lambda_1 \omega_{\text{crit}}^2]$, where ρ is a gain to be defined.

It is possible to define a value of ρ that achieves the phase requirement of the output admittance for $\omega = \omega_{\text{crit}}$. Note that for $\lambda = \lambda_{\text{crit}}$, the real part of $d(z)$ changes sign at $\omega = \omega_{\text{crit}}$. Thus, to satisfy the phase requirement, it is necessary for ρ to take positive values when $\lambda < \lambda_{\text{crit}}$.

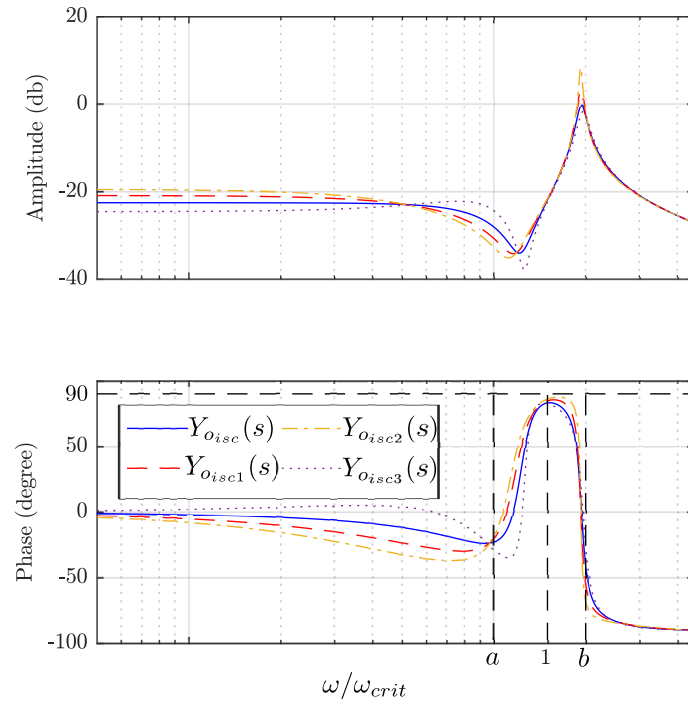
In Figure 8a, the output admittance $\mathbf{Y}_{\text{disc}}(s)$ is shown for $a = \frac{2}{3}$, $b = \frac{4}{3}$, $\varepsilon = 0.5$, $\lambda_1 = 1$, and $\rho = 0.1$. There, the phase requirement in the output admittance is satisfied.

Furthermore, in Figure 8b, the locations of the closed-loop poles when \vec{i}_i , \vec{v}_c , and \vec{i}_s are fed back, are shown in red, for $a = \frac{2}{3}$, $b = \frac{4}{3}$, $\varepsilon = 0.5$, $\lambda_1 = 1$, and $\rho = 0.1$, while varying L_g . As observed, the closed-loop poles remain within the unit circle for all values of L_g .

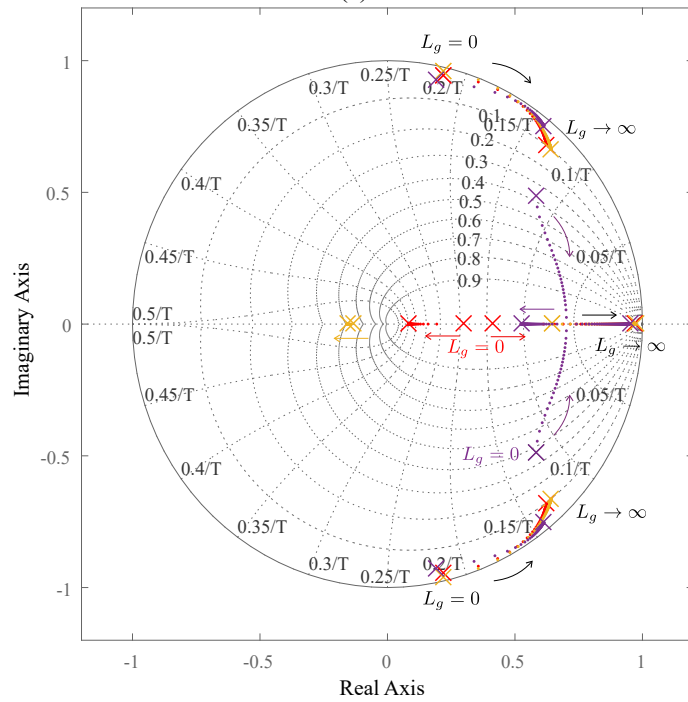
Therefore, by selecting appropriate values of ε , λ_1 , and ρ , it is possible to satisfy the phase requirement for $\mathbf{Y}_o(s)$ and also guarantee the stability of closed-loop poles regardless of the value of L_g .

In addition, Figure 9a illustrates the output admittance $\mathbf{Y}_o(s)$ for different values of k_4 , for the given parameters a , b , ε , λ_1 , and ρ . For all cases the output admittance phase requirement is satisfied. Furthermore, as for $s \rightarrow 0$, $\mathbf{Y}_o(s) \rightarrow \frac{1+k_2+k_4}{k_1+k_3}$, then, it must be satisfied that $k_2 + k_4 > -1$.

On the other hand, Figure 9b presents the variations in the closed-loop poles positions for different values of k_4 , when L_g is varied. It is evident that all the closed-loop poles are situated within the unit circle. Thus, there are small values of k_4 that allow the system to remain stable.



(a)



(b)

Figure 9. (a) Output admittance when \vec{i}_i , \vec{i}_s , \vec{v}_c and \vec{v}_i^* are fed back, for different values of k_4 . $\mathbf{Y}_{oisc}(s)$ corresponds to $k_4 = 0$, $\mathbf{Y}_{oisc1}(s)$ corresponds to $k_4 = 0.2$, $\mathbf{Y}_{oisc2}(s)$ corresponds to $k_4 = 0.4$ and $\mathbf{Y}_{oisc3}(s)$ corresponds to $k_4 = -0.2$. (b) Closed-loop poles location when \vec{i}_i , \vec{v}_c , \vec{i}_s , and \vec{v}_i^* are fed back, using different values of k_4 . The poles are shown for $k_4 = 0.2$ (red), $k_4 = 0.4$ (yellow), and $k_4 = -0.2$ (violet)

By following the outlined gain selection method, it is feasible to guarantee the system stability based on the Nyquist stability criterion for the product of the grid impedance and the output admittance. Additionally, this approach ensures that the closed-loop poles are positioned in stable locations, regardless of variations in the grid inductance value.

4.5 Model extension

Finally, for the case where the effect of phase-locked loop (PLL) on a three-phase system is considered, the proposed model must be extended. The presence of the PLL results in the converter output admittance becoming dq unsymmetric [38], requiring its modeling in synchronous coordinates. The pertinent transfer functions can be transformed into synchronous coordinates, rotating at the grid angular frequency ω_g , by substituting the s -domain variable with $s + j\omega_g$. For this case, the space vectors are represented as column vectors, denoted with the super-index dq . Furthermore, the transfer functions are represented using 2×2 transfer functions matrices, denoted by an overline. This is detailed in Appendix A, along with the PLL dynamics transfer functions matrices.

The block diagram of the linearized model of the grid converter system, incorporating the dynamics of the PLL, is illustrated in Figure 10. Additionally, the PLL dynamics add four variables, $\vec{i}_{iPLL}^{d,q}(z)$, $\vec{v}_{cPLL}^{d,q}(z)$, $\vec{i}_{sPLL}^{d,q}(z)$ and $\vec{v}_{refPLL}^{d,q}(z)$, detailed in Appendix A.

The extent of frequencies impacted by the PLL in the mentioned admittance elements is dictated by the bandwidth of the PLL. For a more in-depth analysis of the influence of the PLL on the converter admittance, the interested reader is directed to [39] and the referenced papers therein.

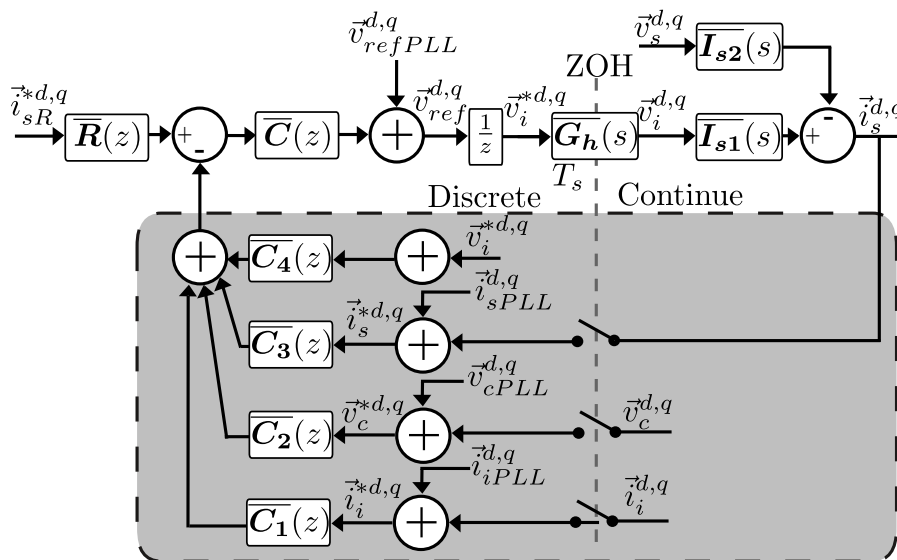


Figure 10. Schematic diagram of the controller with full state feedback, including the dynamics of the PLL.

In this paper, stability is achieved both by satisfying the Nyquist stability criterion between the output admittance and the grid impedance, and by ensuring the closed-loop poles of the system are in stable positions, despite variations in grid impedance. This design overcomes the limitations of the controllers developed in [16, 28, 18], where the system failed to achieve robustness under any type of grid impedance variations.

5. Simulation results

To validate the proposed full state feedback control system, simulations were performed using Matlab/Simulink. The simulation model includes the inverter, LCL filter, and grid modelled as described in previous sections. The parameters used in the simulation are presented in Table 1. Additionally, the DC voltage source v_{dc} was set to 400 V, $a = \frac{2}{3}$ and $b = \frac{4}{3}$.

For this was incorporated a Proportional-Resonant (PR) regulator stage between the reference signal and the output current in the full state feedback system. The PR discrete transfer function, obtained with the Tustin transform method with prewarping [12, 40], is given by

$$PR(z) = k_3 \left[1 + \frac{1}{T_r} \frac{\sin(a_0 \frac{\pi}{3})}{2a_0 \omega_{crit}} \frac{z^2 - 1}{z^2 - 2 \cos(a_0 \frac{\pi}{3}) + 1} \right] \quad (48)$$

where $a_0 = \frac{\omega_0}{\omega_{crit}}$, $\omega_0 = 2\pi 50$, and T_r the resonant time, defined as:

$$T_r = \frac{\theta}{\lambda \omega_{crit}}, \quad (49)$$

being θ is a gain to be defined ($\theta = 10$ in [12, 40]).

Due to the fact that both proportional-integral (PI) and PR regulators can be approximated to a proportional gain at the crossover frequency, when the integral or resonant gain is sufficiently small, they do not affect the stability conditions and were not considered in the stability analysis [12, 15, 41].

Figure 11 shows the output admittance values for both simulated and theoretical cases, considering different values of the gain T_r . Both $Y_{o1}(s)$ and $Y_{o1sim}(s)$ represent the cases with PR for $\theta = 10$, where one corresponds to the theoretical result and the other to the simulated result, respectively. Similarly, $Y_{o2}(s)$ and $Y_{o2sim}(s)$ reflect the cases for $\theta = 1$, also differentiating between theoretical and simulated results. Finally, $Y_{oisc}(s)$ denotes the case without the use of the PR controller. It can be observed that for the case of the PR controllers, there is a phase jump at the resonance frequency $a_0 \omega_{crit}$, for which the output admittance is zero.

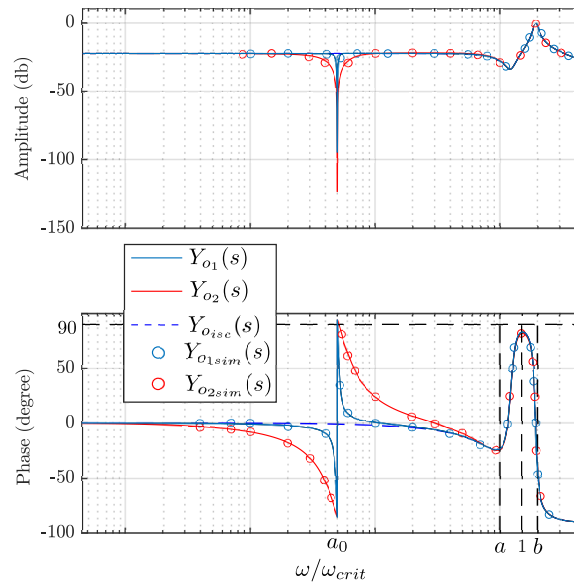


Figure 11. Output admittances for the case in which the states \vec{i}_s , \vec{v}_c and \vec{i}_s are fed back. Both $Y_{o1}(s)$ and $Y_{o1sim}(s)$ represent the cases with PR for $\theta = 10$, with one being the theoretical result and the other the simulated result, respectively. The same applies to $Y_{o2}(s)$ and $Y_{o2sim}(s)$, but for $\theta = 1$. $Y_{oisc}(s)$ represents the case without the use of the PR controller.

Figures 12 and 13 present the step response of the current reference at $t = 0.5$ s for the two previously discussed cases of the PR controllers. In the first case, $\theta = 1$, while in the second case, $\theta = 10$. It is evident that the output current successfully tracks the reference in both scenarios. However, as expected, for $\theta = 10$, the higher gain T_r results in a longer convergence time.

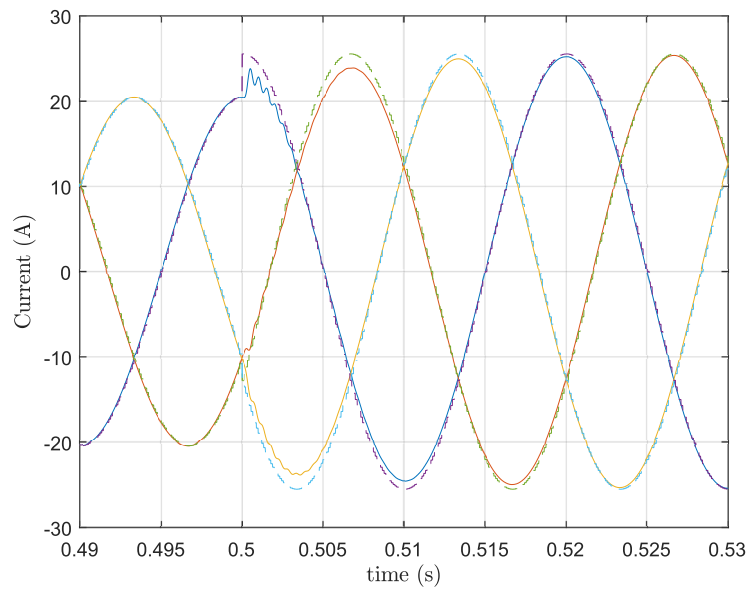


Figure 12. Step response of the output current to a current reference step for the PR controller with $\theta = 1$.

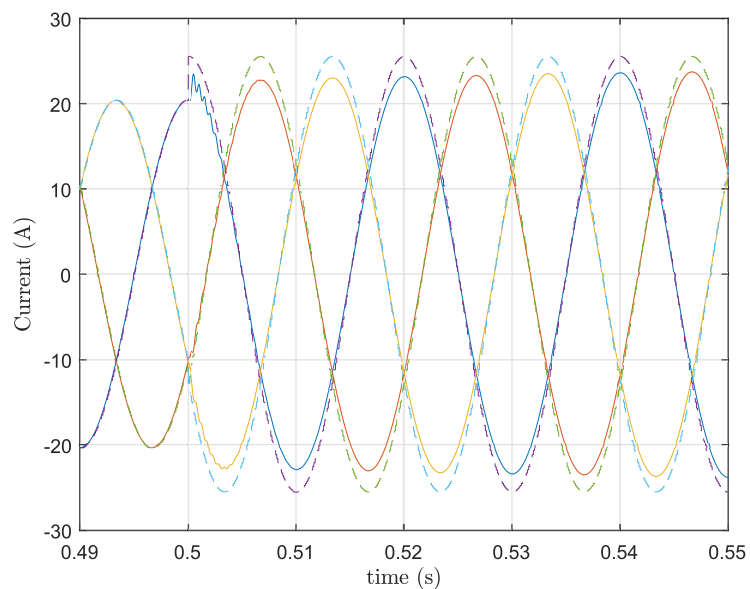


Figure 13. Step response of the output current to a current reference step for the PR controller with $\theta = 10$.

6. Conclusions

This paper presents the analysis of the output impedance modeling of an electronic converter connected to the grid through an LCL filter. The output admittance is calculated as a composition of continuous and discrete signals in the Laplace domain. To ensure system stability, it is necessary that the product between the output admittance and the grid impedance satisfies the Nyquist stability criterion and that the closed-loop poles of the system are in stable positions. By applying the output admittance model to a controller with full state feedback, it is possible to ensure that the output always meets the Nyquist stability criterion. Furthermore, by choosing the correct gain values, the closed-loop poles can be kept in stable positions despite grid inductance variations. This allows the design of a robust controller that remains stable with R-L type grid impedance, satisfying both stability criteria.

This approach surpasses the limitations of other controllers that are not robust against grid impedance variations, as demonstrated by the simulations obtained, which verify the proposed analysis. The system exhibited excellent performance, confirming the effectiveness of the robust controller design.

Appendix A

The inclusion of a synchronous reference frame PLL (SRFPLL) introduces asymmetry into the system, rendering it dq unsymmetric [25]. This unsymmetry results in the representation of complex space vectors using column vectors [38].

$$\vec{i}_s^{d,q} = \begin{bmatrix} i_{sd} \\ i_{sq} \end{bmatrix}, \quad (50)$$

where i_{sd} and i_{sq} represent the d and q components, respectively. Furthermore, the complex transfer functions $\mathbf{Y}_o(s) = \mathbf{Y}_{odd}(s) + j\mathbf{Y}_{oqq}(s)$ are transformed into symmetric transfer function matrices

$$\bar{\mathbf{Y}}_o(s) = \begin{bmatrix} \mathbf{Y}_{odd}(s) & \mathbf{Y}_{odq}(s) \\ \mathbf{Y}_{oqd}(s) & \mathbf{Y}_{oqq}(s) \end{bmatrix}, \quad (51)$$

being, $\mathbf{Y}_{odd}(s) = \mathbf{Y}_{oqq}(s) = \Re\{\mathbf{Y}_o(s)\} = \frac{1}{2} [\mathbf{Y}_o(s) + \mathbf{Y}_o(s)^\dagger]$ and $-\mathbf{Y}_{odq}(s) = \mathbf{Y}_{oqd}(s) = \Im\{\mathbf{Y}_o(s)\} = \frac{1}{2} [\mathbf{Y}_o(s) - \mathbf{Y}_o(s)^\dagger]$, where the superscript \dagger denotes the complex conjugate operation.

Integrating the dynamics of the PLL into the admittance model introduces a dependency on the operating point, necessitating linearization [38]. The dynamic effects of the PLL on the transformed controller variables, \vec{i}_i , \vec{v}_c , \vec{i}_s , \vec{v}_i^* , are expressed as:

$$\vec{i}_{iPLL}^{d,q}(z) = \begin{bmatrix} 0 & -\mathbf{H}_{PLL}(z)i_{iq,0} \\ 0 & \mathbf{H}_{PLL}(z)i_{id,0} \end{bmatrix} \begin{bmatrix} v_{sd}(z) \\ v_{sq}(z) \end{bmatrix}, \quad \vec{v}_{cPLL}^{d,q}(z) = \begin{bmatrix} 0 & -\mathbf{H}_{PLL}(z)v_{cq,0} \\ 0 & \mathbf{H}_{PLL}(z)v_{cd,0} \end{bmatrix} \begin{bmatrix} v_{sd}(z) \\ v_{sq}(z) \end{bmatrix}, \quad (52)$$

$$\vec{i}_{sPLL}^{d,q}(z) = \begin{bmatrix} 0 & -\mathbf{H}_{PLL}(z)i_{sq,0} \\ 0 & \mathbf{H}_{PLL}(z)i_{sd,0} \end{bmatrix} \begin{bmatrix} v_{sd}(z) \\ v_{sq}(z) \end{bmatrix}, \quad \vec{v}_{refPLL}^{d,q}(z) = \begin{bmatrix} 0 & -\mathbf{H}_{PLL}(z)v_{refq,0} \\ 0 & \mathbf{H}_{PLL}(z)v_{refd,0} \end{bmatrix} \begin{bmatrix} v_{sd}(z) \\ v_{sq}(z) \end{bmatrix}, \quad (53)$$

where $i_{id,0}$, $i_{iq,0}$, $v_{cd,0}$, $v_{cq,0}$, $i_{sd,0}$, $i_{sq,0}$, $v_{refd,0}$ and $v_{refq,0}$ are the components values of \mathbf{i}_i , \mathbf{v}_c , \mathbf{i}_s and \mathbf{v}_i at the operating point of the system. The pulse transfer function of the linearized SRF-PLL is expressed in [25] as:

$$\mathbf{H}_{PLL}(z) = \frac{T_s(k_p z + T_s k_i - k_p)}{z^2 + (T_s v_{s,0} k_p - 2)z + T_s v_{c,0}(T_s k_i - k_p) + 1}, \quad (54)$$

where k_p and k_i are the proportional and integral gains of the PLL, and $v_{s,0}$ is the magnitude of the grid voltage vector at the operating point.

Acknowledgements

This paper was partially funded by the Universidad Nacional del Sur (UNS) and the Consejo Nacional de Investigaciones Científicas y Técnicas (CONICET), Argentina.

Conflict of interest statement

The authors declare no conflict of interest.

References

- [1] F. Blaabjerg, R. Teodorescu, M. Liserre, and A. V. Timbus, "Overview of control and grid synchronization for distributed power generation systems," *IEEE Trans. Ind. Electron.*, vol. 53, no. 5, pp. 1398–1409, 2006.
- [2] R. Rosso, X. Wang, M. Liserre, X. Lu, and S. Engelken, "Grid-forming converters: Control approaches, grid-synchronization, and future trends—a review," *IEEE Open J. Ind. Appl.*, vol. 2, pp. 93–109, 2021.
- [3] J. Chhor and C. Sourkounis, "Optimal voltage control strategy for grid-feeding power converters in AC microgrids," *Electric Power Syst. Res.*, vol. 176, p. 105945, 2019.
- [4] H. Wang, J. D. Watson, and N. R. Watson, "A Lyapunov-based nonlinear direct power control for grid-side converters interfacing renewable energy in weak grids," *Electric Power Syst. Res.*, vol. 221, p. 109408, 2023.
- [5] V. Gali, P. K. Jamwal, and N. Gupta, "Stability enhancement of grid side converter in pv-wind-bess based microgrid under weak grid conditions," *Electric Power Syst. Res.*, vol. 221, p. 109481, 2023.
- [6] S. Wang, G. Adam, K. H. Ahmed, and B. Williams, "Comparative evaluation of converter-based compensation schemes for VSC systems to achieve full-range active power transfer in very weak grids," *Electric Power Syst. Res.*, vol. 210, p. 108135, 2022.
- [7] R. Mourouvin, J. C. Gonzalez-Torres, J. Dai, A. Benchaib, D. Georges, and S. Bacha, "Understanding the role of VSC control strategies in the limits of power electronics integration in AC grids using modal analysis," *Electric Power Syst. Res.*, vol. 192, p. 106930, 2021.
- [8] C. Guo, F. Gan, D. Du, Y. Guo, and H. Cheng, "Applicability evaluation of wind farm impedance models using different aggregation methods for high frequency oscillation analysis," *IEEE Trans. Power Deliv.*, vol. 39, no. 4, pp. 2231–2241, 2024.
- [9] F. Benyamina, A. Benrabah, F. Khoucha, M. F. Zia, Y. Achour, and M. Benbouzid, "Online current limiting-based control to improve fault ride-through capability of grid-feeding inverters," *Electric Power Syst. Res.*, vol. 201, p. 107524, 2021.
- [10] R. Pena-Alzola, M. Liserre, F. Blaabjerg, R. Sebastián, J. Dannehl, and F. W. Fuchs, "Analysis of the passive damping losses in LCL-filter-based grid converters," *IEEE Trans. Power Electron.*, vol. 28, no. 6, pp. 2642–2646, 2012.
- [11] R. N. Beres, X. Wang, M. Liserre, F. Blaabjerg, and C. L. Bak, "A review of passive power filters for three-phase grid-connected voltage-source converters," *IEEE J. Emerg. Sel. Topics Power Electron.*, vol. 4, no. 1, pp. 54–69, 2015.
- [12] S. G. Parker, B. P. McGrath, and D. G. Holmes, "Regions of active damping control for LCL filters," *IEEE Trans. Ind. Appl.*, vol. 50, no. 1, pp. 424–432, 2013.
- [13] Y. Tang, P. C. Loh, P. Wang, F. H. Choo, and F. Gao, "Exploring inherent damping characteristic of LCL-filters for three-phase grid-connected voltage source inverters," *IEEE Trans. Power Electron.*, vol. 27, no. 3, pp. 1433–1443, 2011.
- [14] Y. Tang, C. Yoon, R. Zhu, and F. Blaabjerg, "Generalized stability regions of current control for LCL-filtered grid-connected converters without passive or active damping," in *Proc. 2015 IEEE Energy Convers. Congr. Expo. (ECCE)*, Montreal, QC, Canada, Sept. 20–24, 2015, pp. 2040–2047.

- [15] D. Pan, X. Ruan, C. Bao, W. Li, and X. Wang, "Optimized controller design for LCL-type grid-connected inverter to achieve high robustness against grid-impedance variation," *IEEE Trans. Ind. Electron.*, vol. 62, no. 3, pp. 1537–1547, 2014.
- [16] F. M. M. Rahman, U. Riaz, J. Kukkola, M. Routimo, and M. Hinkkanen, "Observer-based current control for converters with an LCL filter: Robust design for weak grids," in *Proc. 2018 IEEE 9th Int. Symp. Sensorless Control Electr. Drives (SLED)*, Helsinki, Sept. 13–14, 2018, pp. 36–41.
- [17] J. M. Gonzalez, C. A. Busada, and J. A. Solsona, "A robust controller for a grid-tied inverter connected through an LCL filter," *IEEE J. Emerg. Sel. Topics Ind. Electron.*, vol. 2, no. 1, pp. 82–89, 2020.
- [18] F. M. Rahman, V. Pirsto, J. Kukkola, M. Routimo, and M. Hinkkanen, "State-space control for LCL filters: Converter versus grid current measurement," *IEEE Trans. Ind. Electron.*, vol. 56, no. 6, pp. 6608–6618, 2020.
- [19] V. Kuruva, V. Thomas, A. H. Abolmasoumi, H.-T. Ngo, and B. Marinescu, "Design and experimental implementation of a robust H_∞ control for LCL grid-connected converter," *IFAC-PapersOnLine*, vol. 58, no. 13, pp. 356–361, 2024.
- [20] J. Sun, "Impedance-based stability criterion for grid-connected inverters," *IEEE Trans. Power Electron.*, vol. 26, no. 11, pp. 3075–3078, 2011.
- [21] Y. Huang, C. Xie, C. Peng, D. Zhou, and J. Zou, "Rethink and design of capacitor-current-feedback active damping for grid-following inverters from a passivity enhancement perspective," *IEEE J. Emerg. Sel. Topics Power Electron.*, vol. 12, no. 3, pp. 2947–2959, 2024.
- [22] C. Wang, X. Wang, Y. He, D. Pan, H. Zhang, X. Ruan, et al., "Passivity-oriented impedance shaping for LCL-filtered grid-connected inverters," *IEEE Trans. Ind. Electron.*, vol. 70, no. 9, pp. 9078–9090, 2023.
- [23] X. Wang, F. Blaabjerg, and W. Wu, "Modeling and analysis of harmonic stability in an ac power-electronics-based power system," *IEEE Trans. Power Electron.*, vol. 29, no. 12, pp. 6421–6432, 2014.
- [24] L. Harnefors, X. Wang, A. G. Yepes, and F. Blaabjerg, "Passivity-based stability assessment of grid-connected VSCs—an overview," *IEEE J. Emerg. Sel. Topics Power Electron.*, vol. 4, no. 1, pp. 116–125, 2015.
- [25] X. Wang, L. Harnefors, and F. Blaabjerg, "Unified impedance model of grid-connected voltage-source converters," *IEEE Trans. Power Electron.*, vol. 33, no. 2, pp. 1775–1787, 2017.
- [26] V. Pirsto, J. Kukkola, M. Hinkkanen, and L. Harnefors, "Intersample modeling of the converter output admittance," *IEEE Trans. Ind. Electron.*, vol. 68, no. 11, pp. 11348–11358, 2020.
- [27] T. Kato, K. Inoue, and Y. Nakajima, "Stabilization of grid-connected inverter system with feed-forward control," in *Proc. 2017 IEEE Energy Convers. Congr. Expo. (ECCE)*, Cincinnati, OH, USA, Oct. 1–5, 2017, pp. 3375–3382.
- [28] J. Kukkola, M. Hinkkanen, and K. Zenger, "Observer-based state-space current controller for a grid converter equipped with an LCL filter: Analytical method for direct discrete-time design," *IEEE Trans. Ind. Electron.*, vol. 51, no. 5, pp. 4079–4090, 2015.
- [29] E. Rodriguez-Diaz, F. D. Freijedo, J. M. Guerrero, J.-A. Marrero-Sosa, and D. Dujic, "Input-admittance passivity compliance for grid-connected converters with an LCL filter," *IEEE Trans. Ind. Electron.*, vol. 66, no. 2, pp. 1089–1097, 2018.
- [30] F. D. Freijedo, M. Ferrer, and D. Dujic, "Multivariable high-frequency input-admittance of grid-connected converters: modeling, validation, and implications on stability," *IEEE Trans. Ind. Electron.*, vol. 66, no. 8, pp. 6505–6515, 2019.
- [31] L. Harnefors, R. Finger, X. Wang, H. Bai, and F. Blaabjerg, "VSC input-admittance modeling and analysis above the nyquist frequency for passivity-based stability assessment," *IEEE Trans. Ind. Electron.*, vol. 64, no. 8, pp. 6362–6370, 2017.
- [32] C. Eckel, D. Babazadeh, and C. Becker, "Classification of converter-driven stability and suitable modeling and analysis methods," *IEEE Access*, vol. 12, pp. 53056–53073, 2024.
- [33] N. Hoffmann, F. W. Fuchs, M. P. Kazmierkowski, and D. Schröder, "Digital current control in a rotating reference frame-part i: System modeling and the discrete time-domain current controller with improved decoupling capabilities," *IEEE Trans. Power Electron.*, vol. 31, no. 7, pp. 5290–5305, 2015.
- [34] S. Buso and P. Mattavelli, "Digital control in power electronics," *Synth. Lect. Power Electron.*, vol. 5, no. 1, pp. 1–229, 2015.
- [35] G. F. Franklin, J. D. Powell, M. L. Workman, *Digital Control of Dynamic Systems*. Menlo Park, CA, USA: Addison-Wesley Reading, 1998, vol. 3.
- [36] J. R. Ragazzini and L. A. Zadeh, "The analysis of sampled-data systems," *Trans. Am. Inst. Electr. Eng., Part II: Appl. Ind.*, vol. 71, no. 5, pp. 225–234, 1952.

- [37] J. Wang, J. D. Yan, L. Jiang, and J. Zou, "Delay-dependent stability of single-loop controlled grid-connected inverters with LCL filters," *IEEE Trans. Power Electron.*, vol. 31, no. 1, pp. 743–757, 2016.
- [38] L. Harnefors, "Modeling of three-phase dynamic systems using complex transfer functions and transfer matrices," *IEEE Trans. Ind. Electron.*, vol. 54, no. 4, pp. 2239–2248, 2007.
- [39] B. Wen, D. Boroyevich, R. Burgos, P. Mattavelli, and Z. Shen, "Analysis of dq small-signal impedance of grid-tied inverters," *IEEE Trans. Power Electron.*, vol. 31, no. 1, pp. 675–687, 2015.
- [40] R. A. Fantino, C. A. Busada, and J. A. Solsona, "Optimum pr control applied to LCL filters with low resonance frequency," *IEEE Trans. Power Electron.*, vol. 33, no. 1, pp. 793–801, 2017.
- [41] D. G. Holmes, T. A. Lipo, B. P. McGrath, and W. Y. Kong, "Optimized design of stationary frame three phase ac current regulators," *IEEE Trans. Power Electron.*, vol. 24, no. 11, pp. 2417–2426, 2009.